

Atomic data and electron-impact broadening effect in DO white dwarf atmospheres: Si VI

R. Hamdi¹, N. Ben Nessib¹, N. Milovanović², L.Č. Popović²,
M.S. Dimitrijević^{2*} and S. Sahal-Bréchet³

¹*Groupe de Recherche en Physique Atomique et Astrophysique, Institut National des Sciences Appliquées et de Technologie, Centre Urbain Nord B. P. No. 676, 1080 Tunis Cedex, Tunisia.*

²*Astronomical observatory, Volgina 7, 11160 Belgrade 74, Serbia.*

³*Laboratoire d'Étude du Rayonnement et de la Matière en Astrophysique, UMR CNRS 8112, Observatoire de Paris-Meudon, 92195 Meudon, France.*

Accepted 1988 December 15. Received 1988 December 14; in original form 1988 October 11

ABSTRACT

Energy levels, electric dipole transition probabilities and oscillator strengths in five times ionized silicon have been calculated in intermediate coupling. The present calculations were carried out with the general purpose atomic-structure program SUPERSTRUCTURE. The relativistic corrections to the non-relativistic Hamiltonian are taken into account through the Breit-Pauli approximation. We have also introduced a semi-empirical correction (TEC) for the calculation of the energy-levels. These atomic data are used to provide semiclassical electron-, proton- and ionized helium- impact line widths and shifts for 15 Si VI multiplet. Calculated results have been used to consider the influence of Stark broadening for DO white dwarf atmospheric conditions.

Key words: atomic data – atomic processes – line: formation – stars: atmospheres – stars: white dwarfs.

1 INTRODUCTION

Atomic data such as transition probabilities (A) play an important role in the diagnostics and modelling of laboratory plasmas (Griem 1974). Various kinetic processes appearing in plasma modelling need reliable knowledge of A values. Further, knowledge of A values gives a possibility for determination of coefficients (B) which characterize the absorption and stimulated emission. These processes are also important in laser physics. The classification of transitions and determination of energy levels are essential parts of the study of a laboratory spectrum. The lack of available atomic data limits our ability to infer reliably the properties of many cosmic plasmas and, hence, address many of the fundamental issues in astrophysics (Savin 2001).

Accurate Stark broadening parameters are important to obtain a reliable modelisation of stellar interiors. The Stark broadening mechanism is also important for the investigation, analysis, and modelling of B-type, and particularly A-type, stellar atmospheres, as well as for white dwarf atmospheres (see e.g. Dimitrijević et al. 2007; Popović et al. 2001).

Silicon, in various ionization stages, is detected in the atmospheres of DO white dwarfs (Werner, Dreizler & Wolff

1995). Si VI lines have been observed as well for example in coronal line regions of planetary nebulae NGC 6302 and 6537 (Casassus, Roche & Barlow 2000).

Uzelac and collaborators (Uzelac et al. 1993) studied plasma broadening of Ne II-Ne VI and F IV-F V experimentally and theoretically, they found that, the results of simplified semiclassical (Griem 1974, Eq 526) calculations show better agreement at higher ionization stages, while the modified semiempirical formula (Dimitrijević & Konjević 1980) seems to be better for the low ionization stages. Unfortunately, due to the lack of atomic data, most of the reported sophisticated semiclassical Stark broadening parameters relate to spectral lines of neutral and low ionization stages. In previous papers (Ben Nessib, Dimitrijević & Sahal-Bréchet 2004; Hamdi et al. 2007), we calculated Stark broadening parameters of quadruply ionized silicon and neon using SUPERSTRUCTURE and Bates & Damgaard (1949) method for oscillator strengths and we found that the difference is tolerable.

Si VI ion belongs to the fluorine-like sequence, its ground state configuration is $1s^2 2s^2 2p^5$ with the term $^2P^\circ$. In this work we present fine-structure energy-levels, transition probabilities and oscillator strengths for Si VI ion. The atomic structure code SUPERSTRUCTURE was used, which allows for configuration interaction, relativistic effects and semi-empirical term energy corrections. Calculated en-

* E-mail: mdimitrijevic@aob.bg.ac.yu

ergies and oscillator strengths are used to provide Stark broadening parameters due to electron, proton, and ionized helium-impact of Si VI lines. The obtained Stark broadening parameters are used to investigate the influence of Stark broadening mechanism in hot, high gravity star atmospheres as for example DO white dwarfs.

2 THE METHOD

In this work, the calculations were carried out with the general-purpose atomic-structure program SUPERSTRUCTURE (Eissner, Jones & Nussbaumer 1974), as modified by Nussbaumer & Storey (1978). The atomic model used to calculate energies of terms or levels and transition probabilities include 26 configurations: $2s^2 2p^5$, $2s 2p^6$, $2s^2 2p^4 3l$, $2s^2 2p^4 4l$, $2s^2 2p^4 5l$, $2s^2 2p^4 6l$, $2s 2p^5 3l$ and $2p^6 3l$ ($l \leq n-1$). Configuration interaction (CI) effects were fully taken into account. The wave functions are of the type

$$\Psi = \sum_i \Phi_i C_i \quad (1)$$

where the basis functions Φ_i are constructed using one-electron orbitals. The latter are calculated with a scaled Thomas-Fermi statistical model potential or obtained from the Coulomb potential. For each radial orbital $P_{nl}(r)$, the potential can be adjusted using a parameter called λ . In the present case, those n and l -dependent scaling parameters λ_{nl} were determined variationally by optimizing the weighted sum of the term energies. The P_{nl} are orthogonalised to each other such that the function $P_{n_1 l}$ is orthogonalised to the function $P_{n_2 l}$ when $n_2 < n_1$. The values adopted for the λ_{nl} parameters are presented in Table A. In this approach the Hamiltonian is taken to be in the form

$$H = H_{nr} + H_{BP} \quad (2)$$

relativistic corrections are included in Breit-Pauli Hamiltonian (H_{BP}) as perturbation to the non relativistic Hamiltonian (H_{nr}). H_{BP} contains the one electron operators for the mass correction, the Darwin contact term, the spin-orbit interaction in the field of the nucleus and the two electron operators for spin-orbit, spin-other orbit, and spin-spin interactions. We also use the so-called term energy corrections (TEC) introduced by Zeippen, Seaton & Morton (1977), in which the Hamiltonian matrix is empirically adjusted to give the best agreement between experimental energies and the final calculated term energies including the relativistic effects. In practice, the TEC for a given term is simply the difference between the calculated and measured energy of the lowest level in the multiplet.

Table A. Optimized parameters λ_{nl} adopted for the 26 configuration model calculation. Positive values for Thomas-Fermi-Dirac potential and negative values for Coulomb potential.

n, l	λ_{nl}	n, l	λ_{nl}	n, l	λ_{nl}	n, l	λ_{nl}
1s	1.4653	4s	1.1091	5d	1.1015	6f	-0.6629
2s	1.1844	4p	1.0960	5f	1.1135	6g	-1.0777
2p	1.1389	4d	1.1103	5g	1.0776	6h	-1.3002
3s	1.1078	4f	1.0478	6s	4.8162		
3p	1.0762	5s	1.1580	6p	6.2669		
3d	1.1808	5p	1.0902	6d	5.3865		

Stark broadening parameter calculations have been performed within the semiclassical perturbation method (Sahal-Bréchet 1969a,b). A detailed description of this formalism with all the innovations is given in Sahal-Bréchet (1969a,b, 1974, 1991); Fleurier, Sahal-Bréchet & Chapelle (1977); Dimitrijević, Sahal-Bréchet & Bommier (1991); Dimitrijević & Sahal-Bréchet (1996). The full halfwidth (w) and shift (d) of an electron-impact broadened spectral line can be expressed as:

$$W = N \int v f(v) dv \left(\sum_{i' \neq i} \sigma_{ii'}(v) + \sum_{f' \neq f} \sigma_{ff'}(v) + \sigma_{el} \right) + W_R$$

$$d = N \int v f(v) dv \int_{R_3}^{R_D} 2\pi \rho d \rho \sin(2\varphi_p) \quad (3)$$

where N is the electron density, $f(v)$ the Maxwellian velocity distribution function for electrons, ρ denotes the impact parameter of the incoming electron, i and f denote the initial and the final atomic energy levels and i' and f' their corresponding perturbing levels, while W_R gives the contribution of the Feshbach resonances (Fleurier, Sahal-Bréchet & Chapelle 1977). The inelastic cross section $\sigma_{ii'}(v)$ can be expressed by an integral over the impact parameter of the transition probability $P_{jj'}(\rho, v)$ as

$$\sum_{j \neq j'} \sigma_{ii'}(v) = \frac{1}{2} \pi R_1^2 + \int_{R_1}^{R_D} 2\pi \rho d \rho \sum_{j \neq j'} P_{jj'}(\rho, v), \quad j = i, f(4)$$

and the elastic cross section is given by

$$\sigma_{el} = 2\pi R_2^2 + \int_{R_2}^{R_D} 2\pi \rho d \rho \sin^2 \delta,$$

$$\delta = (\varphi_p^2 + \varphi_q^2)^{\frac{1}{2}}. \quad (5)$$

The phase shifts φ_p and φ_q due respectively to the polarization potential (r^{-4}) and to the quadrupolar potential (r^{-3}), are given in Section 3 of Chapter 2 in Sahal-Bréchet (1969a) and R_D is the Debye radius. All the cut-offs R_1 , R_2 , R_3 are described in Section 1 of Chapter 3 in Sahal-Bréchet (1969b).

For electrons, hyperbolic paths due to the attractive Coulomb force were used, while for perturbing ions the hyperbolic paths are different since the force is repulsive. The formulae for the ion-impact widths and shifts are analogous to Eqs. (3)-(5), without the resonance contribution to the width.

3 RESULTS AND DISCUSSION

The calculated *ab initio* energies for Si VI are listed in Table 1 along with experimentally determined energies for a number of levels taken from a National Institute of Standards and Technology (NIST) compilation. The configurations for which we present results are $2s^2 2p^5$, $2s 2p^6$, $2s^2 2p^4 3l$, $2s^2 2p^4 4l'$. $l = s, p, d$ and $l' = s, p, d$. We use the LS coupling scheme to designate excited energy.

Two different models are used for the determination of energy levels, the first contains the 9 first configurations of the model given in Sect. 2 and the second contains the total of the 26 configurations. Both 9-configuration model and

more elaborated 26-configuration one give energy levels in good agreement with the NIST values, indeed, our energies are lower than the NIST ones by less than 1% except for the two first excited levels i.e. $2p^5\ ^2P^{\circ}_{1/2}$ and $2s2p^6\ ^2S_{1/2}$. But the results obtained by the second model are always more accurate, that proves the importance of the configuration interaction. Besides, if a term is simply shifted relatively to the ground state, then the difference with observed energy should be essentially constant. In some terms the levels are not always in correct order. For example, the observed order of the levels of $2p^4(^3P)3d\ ^4F$ is (9/2, 7/2, 5/2, 3/2) and the present order is (9/2, 3/2, 5/2, 7/2).

We use the calculated energies and the wavefunctions to calculate oscillator strengths and transition probabilities. With the aim of improving the quality of our wavefunctions, the $2s2p^6\ ^2S_{1/2}$ level is corrected using TEC procedure (see Sect. 2). This method can not be applied for $2p^5\ ^2P^{\circ}_{1/2}$ level. Electric dipole transition probabilities and weighted oscillator strengths are presented in Table 2 for transition with lower level from 1 to 10 and upper level from 3 to 95. The majority of wavelengths are in XUV region. F-like ions are of fundamental importance for current x-ray laser research. Our transition probabilities are compared with NIST values and multiconfiguration Hartree-Fock (MCHF) results of Froese Fischer & Tachiev (2004), who use the observed energies for the calculation of transition probabilities. The agreement is by less than 30% for 70% of strong transitions ($A > 10^8\ s^{-1}$) of NIST compilation. The agreement is much less for weak ones. For weighted oscillator strengths, comparison is made also with Coutinho & Trigueiros (1999) results obtained using multiconfiguration Hartree-Fock relativistic (HFR) approach. In their work the adjusted energy levels were used to optimize the electrostatic parameters, these optimized parameters were used again to calculate the gf-values. In general, our oscillator strengths are in good agreement with the other works except for a few transitions as for example 2-5, 1-6, 2-6, 2-38, for which we observe large disagreement. For the transitions 1-47, 2-48, 2-42 our oscillator strengths agree better with Coutinho & Trigueiros results. On the other hand, for the transitions 2-47, 1-48, 1-56 the agreement with Froese-Fischer & Tachiev values is better. For the transitions 3-15, 1-38, all three methods give different results. The inclusion of a larger number of configurations has an important effect on wavefunctions and A values. TEC correction of the $2s2p^6\ ^2S_{1/2}$ level improve slightly our results. For example for the 2-3 transition our A-value was $1.022E+10\ s^{-1}$ and became $8.840E+09\ s^{-1}$, NIST one is $8.46E+09\ s^{-1}$. The correction of quartet terms do not improve the results.

By combining the SUPERSTRUCTURE code for calculating energy levels and oscillator strengths and the code for the Stark broadening calculations, we calculated Stark broadening parameters. Calculated Stark broadening widths (FWHM) and shifts for a perturber densities of $10^{17}\ cm^{-3}$ and temperatures from 50,000 up to 800,000 K are shown in Table 3 for electron-, proton-, and singly ionized helium impact broadening. Such temperatures are of interest for the modelling and analysis of x-ray spectra, such as the spectra obtained by *Chandra*, modelling of some hot star atmospheres (e.g. DO white dwarf and PG 1195), subphotospheric layers, soft x-ray lasers and laser produced plasmas.

Higher temperatures are of interest for fusion plasma as well as for stellar interiors.

We also specify a parameter C (Dimitrijević & Sahal-Bréchet 1984), which gives an estimate for the maximal perturber density for which the line may be treated as isolated, when it is divided by the corresponding full width at half maximum. For each value given in Table 3 the collision volume V multiplied by the perturber density N is much less than one and the impact approximation is valid (Sahal-Bréchet 1969a,b). When the impact approximation is not valid, the ion broadening contribution may be estimated by using the quasistatic approach (Griem 1974; Sahal-Bréchet 1991; Ben Nessib, Ben Lakhdar & Sahal-Bréchet 1996).

Unfortunately, no experimental data are yet available for the Stark broadening parameters so that the comparison is made only with Dimitrijević's (1993) results obtained using the modified semiempirical formula (Dimitrijević & Konjević 1980). All our values are greater than Dimitrijević's ones. The ratio $\frac{w_e}{w_{MSE}}$ shows in average an agreement within 56%. Low disagreements are usually found for resonance lines, for example for the spectral line $2p^5\ ^2P^{\circ}-2p^4(^3P)3s\ ^2P$ ($\lambda = 100,2\ \text{\AA}$) the ratio $\frac{w_e}{w_{MSE}}$ is only 1.06 for $T = 800,000\ K$.

4 STARK BROADENING EFFECT IN WHITE DWARF ATMOSPHERES

White dwarfs are separated in two distinct spectroscopic sequences, the DA and non-DA white dwarfs. The former ones display a pure hydrogen (optical) spectrum. The second, helium-rich sequence comprise DO ($T_{eff} > 45,000\ K$), DB ($11,000 < T_{eff} < 30,000\ K$) and DC ($T_{eff} < 11,000\ K$) white dwarfs. At the highest effective temperatures the DOs are connected to the helium, carbon and oxygen-rich PG 1159.

Silicon in various ionization stages is present DO white dwarf atmospheres (Werner, Dreizler & Wolff 1995). We used our results for Stark widths to examine the importance of electron-impact broadening in atmospheres of DO white dwarfs for a trace element like Si VI. Model atmospheres were taken from Wesemael (1981).

In hot star atmospheres, besides electron-impact broadening (Stark broadening) the important broadening mechanism is a Doppler (Thermal) one as well as the broadening due to the turbulence and stellar rotation. Other types of spectral line broadening, such as van der Waals, resonance and natural broadening, are usually negligible. For a Doppler-broadened spectral lines, the intensity distribution is not Lorentzian as for electron impact broadening but Gaussian, whose full half width of the spectral lines may be determined by the equation (see e.g. Konjević 1999)

$$w_D[\text{\AA}] = 7.16 \times 10^{-7} \lambda[\text{\AA}] \sqrt{\frac{T[K]}{M_{Si}}} \quad (6)$$

where atomic weight for silicon is $M_{Si} = 28.1\ a.u.$

The importance of Stark broadening in stellar atmospheres is illustrated in Figs 1-4. In Fig 1 Stark (FWHM) and Doppler widths for Si VI $2p^4(^3P)3s\ ^2P-2p^4(^3P)3p\ ^2D^{\circ}$ ($\lambda = 1226,7\ \text{\AA}$) spectral line as a function of atmospheric layer temperatures are shown. Stark widths are shown for

6 atmospheric models with effective temperature $T_{eff}=50,000$ K-100,000 K and logarithm of surface gravity $\log g=8$. We can see in Fig 1. that Stark broadening is more important than Doppler broadening for deeper atmospheric layers for all effective temperatures. For WD with effective temperature $T_{eff}=50,000$ K, Stark and Doppler widths are equal for temperature layer $T\approx 70,000$ K and for WD with effective temperature $T_{eff}=100,000$ K, Stark and Doppler are equal for temperature layer $T\approx 125,000$ K. One should take into account however, that even when the Doppler width is larger than Stark width, due to different behaviour of Gaussian and Lorentzian distributions, Stark broadening may be important in line wings. In Fig 2. we present Stark (FWHM) and Doppler widths for Si VI ($\lambda = 1226,7$ Å) spectral line as a function of Rosseland optical depth for the same atmospheric models as in Fig 1.

The dependence of Stark and Doppler broadening in atmospheric layer temperature for 4 values of surface gravity is shown in Fig 3. Atmospheric models used here have effective temperature $T_{eff}=80,000$ K. For stellar atmosphere with higher values of surface gravity ($\log g = 8-9$), Stark broadening is significantly larger than Doppler one. For stellar atmosphere with surface gravity $\log g = 7$, Stark widths are comparable to Doppler widths only for deeper hot atmospheric layer. For stellar atmospheres with $\log g = 6$, Doppler broadening is dominant for all atmospheric layers.

5 CONCLUSIONS

In present work we have calculated *ab initio* energy levels for the eight lowest configurations of Si VI. We have also calculated transition probabilities and oscillator strengths for 288 transitions. These data are useful for interpretation of laboratory and astrophysical spectra, since, the reliability of the predicted emergent spectra and the derived spectral diagnoses is directly influenced by the quality of radiative data. The method used here is semirelativistic one, the relativistic corrections are included by using the Breit-Pauli Hamiltonian as perturbation to the non relativistic Hamiltonian. To make fully relativistic calculation, the GRASP code (Dyall et al. 1989) can be used. One should note also that Martin & Wiese (1976) investigated the influence of relativistic effects on the oscillator strength values for the lithium isoelectronic sequences and found that the influence is not important on investigated f values for the ionization degrees investigated in our work. We have reported results of Stark broadening parameter calculations for 15 spectral lines of Si VI. For the simple spectrum, the Stark broadening parameters of different lines are nearly the same within a multiplet (Wiese & Konjević 1992). Consequently, we have used the averaged atomic data for a multiplet as a whole and calculate the corresponding Stark widths and shifts. We see that using the SUPERSTRUCTURE code one obtains a set of energy levels and oscillator strengths, enabling a calculation of Stark broadening parameters when other theoretical and experimental data do not exist. The Stark broadening parameters obtained here, contribute to the creation of a set of such data for as large as possible number of spectral lines, of significance for a number of problems in astrophysical, laboratory and technological plasma research. Our analysis of the influence of Stark broadening on Si VI ($\lambda = 1226,7$

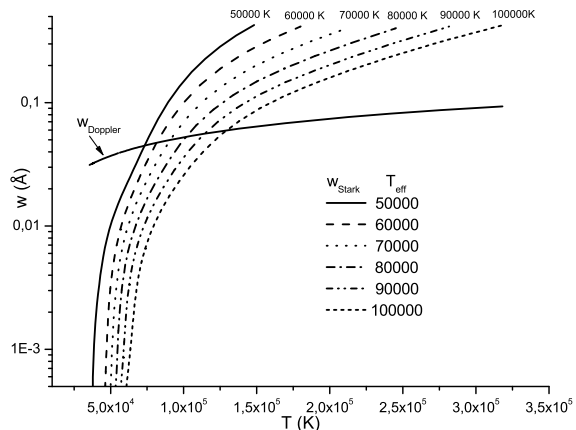


Figure 1. Stark and Doppler widths for Si VI $2p^4(^3P)3s^2P-2p^4(^3P)3p^2D^\circ$ ($\lambda=1226,7$ Å) spectral line as a function of atmospheric layer temperatures. Stark widths are shown for 6 atmospheric models with effective temperature $T_{eff}=50,000$ K-100,000 K and $\log g=8$.

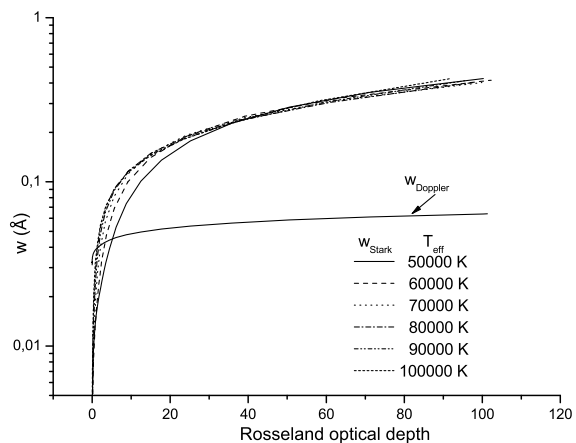


Figure 2. Stark and Doppler widths for Si VI $2p^4(^3P)3s^2P-2p^4(^3P)3p^2D^\circ$ ($\lambda=1226,7$ Å) spectral line as a function of Rosseland optical depth. Stark widths are shown for 6 atmospheric models with effective temperature $T_{eff}=50,000$ K-100,000 K and $\log g=8$.

Å) spectral line for stellar plasma conditions, demonstrates the importance of this broadening mechanism for hot, high gravity star atmospheres as for example DO white dwarfs.

ACKNOWLEDGMENTS

We would like to thank C.J. Zeippen for providing his version of SUPERSTRUCTURE code. This work is a part of the projects 146001 "Influence of collisional processes on astrophysical plasma line shapes" and 146002 "Astrophysical Spectroscopy of Extragalactic Objects" supported by the Ministry of Science of Serbia.

Table 1. Energy levels for Si VI in cm^{-1} . Key: a number assigned to each level. *LS*: *LS* term and parity (superscript $^{\circ}$ designate an odd level). *J*: *J* value of the level. E_{9-conf} : *ab initio* energy levels, calculated with 9-configuration model. $E_{26-conf}$: *ab initio* energy levels, calculated with 26-configuration model. E_{NIST} : NIST values.

Key	configuration	LS	J	E_{9-conf}	$E_{26-conf}$	E_{NIST}
1	$2p^5$	$2P^{\circ}$	3/2	0	0	0
2			1/2	2796	2839	5090
3	$2s2p^6$	$2S$	1/2	435632	426462	406497
4	$2p^4(^3P)3s$	$4P$	5/2	971851	982366	990516
5			1/2	975520	986496	995470
6			3/2	975969	987021	993640
7	$2p^4(^3P)3s$	$2P$	3/2	987370	999127	1005430
8			1/2	987692	999494	1009118
9	$2p^4(^1D)3s$	$2D$	5/2	1024374	1036129	1041416
10			3/2	1024884	1036533	1041472
11	$2p^4(^3P)3p$	$4P^{\circ}$	3/2	1052168	1061210	1069854
12			5/2	1052404	1061401	1068813
13			1/2	1053583	1062874	1071129
14	$2p^4(^3P)3p$	$4D^{\circ}$	7/2	1059089	1070621	1078935
15			1/2	1061265	1073242	1083003
16			3/2	1062447	1074609	1082215
17			5/2	1062788	1074942	1080700
18	$2p^4(^3P)3p$	$2D^{\circ}$	5/2	1068139	1080203	1086796
19			3/2	1068477	1080547	1089547
20	$2p^4(^3P)3p$	$2P^{\circ}$	1/2	1077264	1080958	
21			3/2	1075947	1084287	1092171
22	$2p^4(^1S)3s$	$2S$	1/2	1071075	1084295	1094449
23	$2p^4(^3P)3p$	$4S^{\circ}$	3/2	1074673	1087671	1093752
24	$2p^4(^3P)3p$	$2S^{\circ}$	1/2	1094162	1088558	
25	$2p^4(^1D)3p$	$2F^{\circ}$	5/2	1106342	1118373	1123540
26			7/2	1106472	1118689	1124219
27	$2p^4(^1D)3p$	$2D^{\circ}$	3/2	1116033	1128816	1134081
28			5/2	1116641	1129460	1134496
29	$2p^4(^1D)3p$	$2P^{\circ}$	3/2	1140823	1145932	1147901
30			1/2	1140921	1145980	1150282
31	$2p^4(^1S)3p$	$2P^{\circ}$	3/2	1182143	1171561	
32			1/2	1182942	1172417	
33	$2p^4(^3P)3d$	$4D$	7/2	1161013	1172209	1181167
34			5/2	1162025	1173271	1181649
35			3/2	1162165	1173376	1182311
36			1/2	1162754	1173979	1182894
37	$2p^4(^3P)3d$	$4F$	9/2	1169569	1182612	1189844
38			3/2	1171689	1184525	1194327
39			5/2	1172030	1184838	1193223
40			7/2	1172047	1184946	1191541
41	$2p^4(^3P)3d$	$4P$	1/2	1176385	1188594	1194899
42			3/2	1177207	1189543	1195984
43			5/2	1178908	1191510	1197727
44	$2p^4(^3P)3d$	$2F$	7/2	1177148	1189950	1194987
45			5/2	1178364	1190848	1197151
46	$2p^4(^3P)3d$	$2P$	1/2	1182736	1194144	1200710
47			3/2	1185454	1196939	1204740
48	$2p^4(^3P)3d$	$2D$	3/2	1185167	1195061	1201100
49			5/2	1185973	1196247	1202960
50	$2p^4(^1D)3d$	$2G$	7/2	1214568	1227449	
51			9/2	1214715	1227538	1232671
52	$2p^4(^1D)3d$	$2S$	1/2	1223636	1234097	1239190
53	$2p^4(^1D)3d$	$2P$	3/2	1224780	1234806	1241050
54			1/2	1225778	1235883	1242390
55	$2p^4(^1D)3d$	$2F$	7/2	1223872	1236910	1242649
56			5/2	1223946	1236950	1242186
57	$2p^4(^1D)3d$	$2D$	5/2	1226710	1237621	1243020
58			3/2	1227611	1238313	1243860

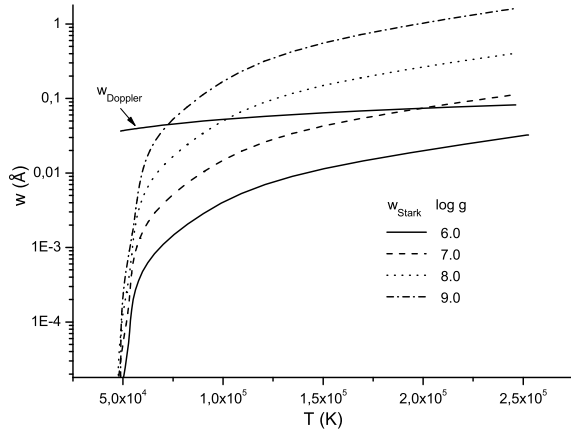


Figure 3. Stark and Doppler widths for Si VI $2p^4(^3P)3s\ ^2P-2p^4(^3P)3p\ ^2D^o$ ($\lambda=1226,7\ \text{\AA}$) spectral line as a function of atmospheric layer temperatures. Stark widths are shown for 4 values of model gravity $\log g = 6-9$, $T_{eff} = 80,000\ \text{K}$.

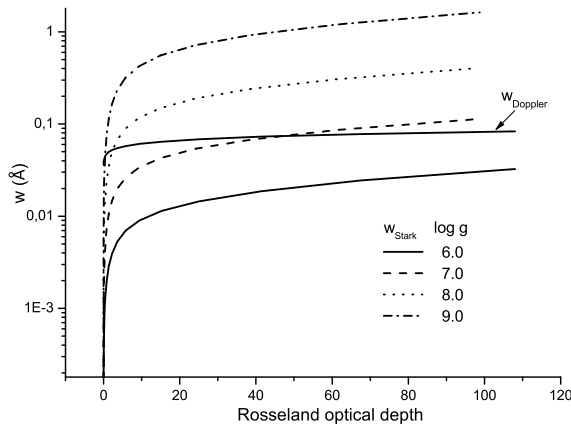


Figure 4. Stark and Doppler widths for Si VI $2p^4(^3P)3s\ ^2P-2p^4(^3P)3p\ ^2D^o$ ($\lambda=1226,7\ \text{\AA}$) spectral line as a function of Rosseland optical depth. Stark widths are shown for 4 values of model gravity $\log g = 6-9$, $T_{eff} = 80,000\ \text{K}$.

REFERENCES

- Bates D.R., Damgaard A., 1949, *Philos. Trans. R. Soc. London A*, 242, 101
 Ben Nessib N., Ben Lakhdar Z., Sahal-Br echot S., 1996, *Phys. Scr.*, 54, 608
 Ben Nessib N., Dimitrijević M.S., Sahal-Br echot S., 2004, *A&A*, 423, 397
 Casassus S., Roche P.F., Barlow M.J., 2000, *MNRAS*, 314, 657
 Coutinho L.H., Trigueiros A.G., 1999, *ApJS*, 121, 591
 Dimitrijević M.S., 1993, *A&AS*, 100, 237
 Dimitrijević M.S., Konjević N., 1980, *J. Quant. Spectrosc. Radiat. Transfer*, 24, 451
 Dimitrijević M.S., Ryabchikova T., Simić Z., Popović L. Č., Đaćić M., 2007, *A&A*, 469, 681

- Dimitrijević M.S., Sahal-Br echot S., 1984, *J. Quant. Spectrosc. Radiat. Transfer*, 31, 301
 Dimitrijević M.S., Sahal-Br echot S., 1996, *Phys. Scr.*, 54, 50
 Dimitrijević M.S., Sahal-Br echot S., Bommier V., 1991, *A&AS*, 89, 581
 Dylla K.G., Grant I.P., Johnson C.T., Parpia, F.A., Plummer, E.P., 1989, *Comput. Phys. Commun.*, 55, 424
 Eissner W., Jones M., Nussbaumer H., 1974, *Comput. Phys. Commun.*, 8, 270
 Fleurier C., Sahal-Br echot S., Chapelle J., 1977, *J. Quant. Spectrosc. Radiat. Transfer*, 17, 595
 Froese Fischer C., Tachiev G., 2004, *At. Data Nucl. Data Tables*, 87, 1
 Griem H.R., 1974, *Spectral line Broadening by Plasmas*. McGraw-Hill, New York
 Hamdi R., Ben Nessib N., Dimitrijević M.S., Sahal-Br echot S., 2007, *ApJS*, 170, 243
 Konjević N., 1999, *Phys. Rep.*, 316, 339
 Konjević N., 1999, *Phys. Rep.*, 316, 339
 Martin G. A., Wiese, W. L., 1976, *J. Phys. Chem. Ref. Data*, 5, 537
 Nussbaumer H., Storey J.P., 1978, *A&A*, 64, 139
 Popović L. Č., Simić S., Milovanović N., Dimitrijević M.S., 2001, *ApJS*, 135, 109
 Sahal-Br echot S., 1969a, *A&A*, 1, 91
 Sahal-Br echot S., 1969b, *A&A*, 2, 322
 Sahal-Br echot S., 1974, *A&A*, 35, 319
 Sahal-Br echot S., 1991, *A&A*, 245, 322
 Savin D.W., 2001, in Ferland G., Savin D.W., eds., *ASP Conference Series 247, Spectroscopic Challenges of Photoionized Plasmas*, p. 167
 Uzelac N.I., Glenzer S., Konjević N., Hey J.D., Kunze H.J., 1993, *Phys. Rev. E*, 47, 3623
 Werner K., Dreizler S., Wolf B., 1995, *A&A*, 298, 567
 Wesemael F., 1981, *ApJS*, 45, 177
 Wiese W.L., Konjević N., 1992, *J. Quant. Spectrosc. Radiat. Transfer*, 47, 185
 Zeippen C.J., Seaton M.J., Morton D.C., 1977, *MNRAS*, 181, 527

This paper has been typeset from a $\text{\TeX}/\text{\LaTeX}$ file prepared by the author.

Table 1. *continued.*

<i>Key</i>	<i>configuration</i>	<i>LS</i>	<i>J</i>	E_{9-conf}	$E_{26-conf}$	E_{NIST}
59	$2p^4(1S)3d$	2D	3/2	1290487	1280925	1291790
60			5/2	1291154	1281640	1291510
61	$2p^4(3P)4s$	4P	5/2	1302866	1314745	
62			1/2	1305283	1317544	
63			3/2	1306890	1319305	
64	$2p^4(3P)4s$	2P	3/2	1308844	1321429	1329900
65			1/2	1310323	1323045	
66	$2p^4(3P)4p$	$^4P^\circ$	5/2	1333771	1340871	
67			3/2	1333474	1340979	
68			1/2	1334815	1342729	
69	$2p^4(3P)4p$	$^4D^\circ$	7/2	1335203	1347589	
70			1/2	1337989	1350092	
71			3/2	1338555	1351294	
72			5/2	1338545	1352144	
73	$2p^4(3P)4p$	$^2D^\circ$	5/2	1339973	1351228	
74			3/2	1339638	1352195	
75	$2p^4(3P)4p$	$^2S^\circ$	1/2	1340521	1352722	
76	$2p^4(3P)4p$	$^4S^\circ$	3/2	1342995	1355616	
77	$2p^4(3P)4p$	$^2P^\circ$	3/2	1349411	1359114	
78			1/2	1349310	1359465	
79	$2p^4(1D)4s$	2D	5/2	1352262	1365126	1371820
80			3/2	1352767	1365515	
81	$2p^4(3P)4d$	4D	7/2	1371226	1382797	
82			5/2	1372174	1384161	
83			3/2	1372430	1384614	
84			1/2	1373107	1385519	
85	$2p^4(3P)4d$	4F	9/2	1374444	1387108	
86			7/2	1376125	1388760	
87			5/2	1376654	1389343	
88			3/2	1376461	1389348	
89	$2p^4(3P)4d$	4P	1/2	1377931	1390631	
90			3/2	1379041	1391893	
91			5/2	1380830	1393884	
92	$2p^4(3P)4d$	2F	5/2	1380128	1392885	
93			7/2	1380477	1393669	
94	$2p^4(3P)4d$	2P	1/2	1381851	1393521	1402490
95			3/2	1384583	1396287	1403050
96	$2p^4(3P)4d$	2D	3/2	1385040	1395603	
97			5/2	1385544	1396797	1404870
98	$2p^4(3P)4p$	$^2F^\circ$	7/2	1382852	1395696	
99			5/2	1382929	1395739	
100	$2p^4(1D)4p$	$^2D^\circ$	3/2	1386127	1399126	
101			5/2	1386673	1399653	
102	$2p^4(1D)4p$	$^2P^\circ$	1/2	1392385	1405752	
103			3/2	1392362	1405797	
104	$2p^4(1D)4s$	2S	1/2	1419675	1432175	
105	$2p^4(1D)4d$	2G	7/2	1421515	1434310	
106			9/2	1421617	1434434	
107	$2p^4(1D)4d$	2P	3/2	1424977	1436510	
108			1/2	1425973	1437711	
109	$2p^4(1D)4d$	2F	7/2	1424368	1437280	
110			5/2	1424453	1437401	
111	$2p^4(1D)4d$	2D	5/2	1425961	1438109	1444340
112			3/2	1426992	1438858	1445010
113	$2p^4(1D)4d$	2S	1/2	1427833	1440235	
114	$2p^4(1S)4p$	$^2P^\circ$	1/2	1453543	1466060	
115			3/2	1453658	1466257	
116	$2p^4(1S)4d$	2D	3/2	1493396	1506902	
117			5/2	1494092	1507702	

Table 2. Transition probabilities (A_{ki}), calculated wavelengths (λ) and weighted oscillator strengths (gf) for Si VI spectrum. present : this work, FF: Froese Fischer & Tachiev (2004), CT: Coutinho & Trigueiros (1999). The numbers in brackets denote powers of ten.

<i>Transition</i>	$\lambda(\text{\AA})$	$A_{ki}(s^{-1})$			gf			
		<i>present</i>	<i>FF</i>	<i>NIST</i>	<i>present</i>	<i>FF</i>	<i>NIST</i>	<i>CT</i>
1 – 3	246.004	1.805(10)	1.777(10)	1.77(10)	3.275(-01)	3.210(-01)	3.206(-01)	4.04(-01)
2 – 3	247.734	8.840(09)	8.517(09)	8.46(09)	1.627(-01)	1.576(-01)	1.573(-01)	2.00(-01)
1 – 4	101.795	8.982(07)	7.405(07)	7.51(07)	8.372(-04)	6.784(-04)	6.886(-04)	8.00(-04)
1 – 5	101.369	1.340(09)	8.423(06)	8.55(06)	4.128(-03)	2.547(-05)	2.588(-05)	
2 – 5	101.661	2.010(09)	2.624(08)	2.64(08)	6.229(-03)	8.016(-04)	8.072(-04)	9.00(-04)
1 – 6	101.315	1.019(08)	1.167(09)	1.18(09)	6.270(-04)	7.088(-03)	7.161(-03)	7.50(-03)
2 – 6	101.607	9.716(06)	1.010(08)	1.08(08)	6.016(-05)	6.194(-04)	6.266(-04)	6.00(-04)
1 – 7	100.087	6.667(10)	6.753(10)	6.74(10)	4.005(-01)	4.004(-01)	3.999(-01)	4.88(-01)
2 – 7	100.373	1.292(10)	1.098(10)	1.09(10)	7.803(-02)	6.574(-02)	6.561(-02)	7.90(-02)
1 – 8	100.051	2.509(10)	2.823(10)	2.82(10)	7.530(-02)	8.304(-02)	8.317(-02)	1.02(-01)
2 – 8	100.336	4.987(10)	5.156(10)	5.15(10)	1.505(-01)	1.532(-01)	1.531(-01)	1.86(-01)
1 – 9	96.513	3.189(10)	3.087(10)	3.08(10)	2.672(-01)	2.556(-01)	2.558(-01)	
1 – 10	96.475	4.625(09)	3.056(09)	3.03(09)	2.582(-02)	1.687(-02)	1.674(-02)	2.03(-02)
2 – 10	96.740	2.674(10)	2.796(10)	2.79(10)	1.501(-01)	1.558(-01)	1.559(-01)	1.94(-01)
3 – 11	152.739	1.064(05)	7.895(05)		1.488(-06)	1.077(-05)		
4 – 11	1268.336	3.944(08)	4.159(08)	4.11(08)	3.805(-01)	3.935(-01)	3.908(-01)	
5 – 11	1338.445	1.569(08)	1.624(08)	1.62(08)	1.685(-01)	1.746(-01)	1.749(-01)	1.89(-01)
6 – 11	1347.907	8.664(07)	9.855(07)	9.73(07)	9.440(-02)	1.010(-01)	1.004(-01)	1.07(-01)
7 – 11	1610.745	4.125(05)	5.789(04)	5.56(04)	6.418(-04)	8.312(-05)	8.035(-05)	
8 – 11	1620.320	1.353(07)	3.677(03)	3.79(03)	2.130(-02)	5.938(-06)	6.165(-06)	
9 – 11	3987.165	6.968(04)	1.627(04)	1.62(04)	6.643(-04)	1.218(-04)	1.199(-04)	
10 – 11	4052.352	7.466(03)	5.228(03)	5.44(03)	7.353(-05)	3.929(-05)	4.036(-05)	
4 – 12	1265.271	5.940(08)	5.712(08)	5.64(08)	8.554(-01)	8.322(-01)	8.279(-01)	8.72(-01)
6 – 12	1344.446	9.628(07)	1.104(08)	1.10(08)	1.565(-01)	1.744(-01)	1.753(-01)	1.91(-01)
7 – 12	1605.805	1.630(06)	2.988(05)	3.09(05)	3.781(-03)	6.648(-04)	6.918(-04)	
9 – 12	246.004	1.458(05)	2.110(03)	2.37(03)	2.054(-03)	2.554(-05)	2.837(-05)	
10 – 12	247.734	3.719(01)	2.179(02)	2.40(02)	5.410(-07)	2.646(-06)	2.890(-06)	
3 – 13	101.795	2.939(05)	4.160(05)		2.046(-06)	2.628(-06)		
5 – 13	1309.272	3.686(07)	7.502(07)	7.46(07)	1.894(-02)	3.900(-02)	3.899(-02)	
6 – 13	1318.325	5.969(08)	5.915(08)	5.85(08)	3.111(-01)	2.933(-01)	2.917(-01)	3.10(-01)
7 – 13	1568.682	1.079(06)	8.921(05)	9.49(05)	7.964(-04)	6.160(-04)	6.606(-04)	
8 – 13	1577.761	1.707(06)	4.217(05)	4.38(05)	1.274(-03)	3.268(-04)	3.419(-04)	
10 – 13	3796.252	1.573(04)	1.490(04)	1.49(04)	6.798(-05)	5.128(-05)	5.018(-05)	
4 – 14	1133.080	1.056(09)	1.033(09)	1.03(09)	1.626(+00)	1.581(+00)	1.577(+00)	1.71(+00)
9 – 14	2899.222	6.193(03)	3.205(03)	3.54(03)	6.244(-05)	2.776(-05)	3.019(-05)	
3 – 15	149.982	5.880(04)	1.367(06)	1.40(06)	3.966(-07)	8.972(-06)	9.141(-06)	9.00(-05)
5 – 15	1152.795	9.112(08)	8.776(08)	8.74(08)	3.631(-01)	3.426(-01)	3.419(-01)	3.70(-01)
6 – 15	1159.808	6.171(07)	1.290(08)	1.29(08)	2.489(-02)	4.836(-02)	4.841(-02)	
7 – 15	1349.252	9.550(05)	2.566(05)	2.58(05)	5.213(-04)	1.278(-04)	1.228(-04)	
8 – 15	1355.964	1.964(07)	7.280(05)	7.09(05)	1.083(-02)	3.998(-04)	3.899(-04)	
10 – 15	2724.120	6.668(04)	8.238(03)		1.484(-04)	1.454(-05)		
3 – 16	149.675	3.954(05)	5.543(05)	5.73(05)	5.312(-06)	7.292(-06)	7.516(-06)	
4 – 16	1084.091	2.953(07)	2.000(07)	2.03(07)	2.081(-02)	1.423(-02)	1.452(-02)	
5 – 16	1134.903	4.668(08)	4.842(08)	4.82(08)	3.606(-01)	3.850(-01)	3.837(-01)	4.13(-01)
6 – 16	1141.699	5.093(08)	4.957(08)	4.95(08)	3.981(-01)	3.781(-01)	3.768(-01)	4.11(-01)
7 – 16	1324.806	1.466(06)	1.213(03)	1.88(03)	1.543(-03)	1.232(-06)	1.909(-06)	
8 – 16	1331.276	2.832(07)	4.541(06)	4.53(06)	3.010(-02)	5.094(-03)	5.081(-03)	
9 – 16	2598.741	7.183(04)	8.858(03)	9.91(03)	2.909(-04)	3.241(-05)	3.572(-05)	
10 – 16	2626.277	1.035(02)	1.337(04)	1.45(04)	4.281(-07)	4.908(-05)	5.236(-05)	
4 – 17	1080.192	2.103(08)	1.903(08)	1.91(08)	2.207(-01)	2.100(-01)	2.113(-01)	2.38(-01)
6 – 17	1137.375	8.616(08)	7.873(08)	7.83(08)	1.003(+00)	9.320(-01)	9.289(-01)	9.98(-01)
7 – 17	1318.987	7.133(06)	1.864(07)	1.86(07)	1.116(-02)	2.957(-02)	2.958(-02)	
9 – 17	2576.446	2.564(03)	8.978(03)	9.31(03)	1.531(-05)	5.316(-05)	5.432(-05)	
4 – 18	1022.110	5.562(05)	1.307(07)	1.33(07)	5.227(-04)	1.265(-02)	1.285(-02)	
6 – 18	1073.164	1.749(07)	2.238(07)	2.22(07)	1.811(-02)	2.313(-02)	2.301(-02)	

Table 2. Continued.

Transition	$\lambda(\text{\AA})$	$A_{ki}(s^{-1})$			gf			
		present	FF	NIST	present	FF	NIST	CT
7 – 18	1233.405	8.506(08)	8.032(08)	8.02(08)	1.164(+00)	1.090(-01)	1.088(+00)	
9 – 18	2268.921	7.863(04)	2.465(05)	2.49(05)	3.641(-04)	1.090(-03)	1.086(-03)	
10 – 18	2289.882	1.355(02)	6.522(03)	6.85(03)	6.391(-07)	2.892(-05)	2.999(-05)	
3 – 19	148.357	2.047(06)	1.279(07)		2.702(-05)	1.645(-04)		
4 – 19	1018.526	8.703(06)	2.181(06)	2.75(06)	5.415(-03)	1.326(-03)	1.336(-03)	
5 – 19	1063.250	9.488(07)	2.892(06)		6.433(-02)	1.952(-03)	1.862(-03)	
6 – 19	1063.250	1.100(05)	1.283(06)	1.22(06)	7.545(-05)	8.336(-04)	7.961(-04)	
7 – 19	1228.189	9.754(07)	4.377(08)	4.54(08)	8.824(-02)	3.701(-01)	3.845(-01)	3.66(-01)
8 – 19	1233.748	6.973(08)	3.698(08)	3.48(08)	6.365(-01)	3.420(-01)	3.221(-01)	
9 – 19	2251.333	3.457(05)	6.305(06)	7.30(06)	1.051(-03)	1.648(-02)	1.887(-02)	
10 – 19	2271.969	4.466(04)	2.421(06)	2.63(06)	1.382(-04)	6.344(-03)	6.807(-03)	
3 – 20	148.267	1.378(08)	8.949(07)		9.085(-04)	5.760(-04)		
5 – 20	1058.626	6.333(06)	1.717(05)		2.128(-04)	5.804(-05)		
6 – 20	1064.537	6.918(06)	1.331(06)		2.351(-03)	4.332(-04)		
7 – 20	1222.023	5.861(08)	6.643(08)		2.624(-01)	2.813(-01)		
8 – 20	1227.526	6.666(07)	5.304(07)		3.012(-02)	2.458(-02)		
10 – 20	2250.959	2.878(07)	2.829(07)		4.373(-02)	3.719(-02)		
3 – 21	147.538	1.880(08)	1.114(08)	1.10(08)	2.454(-03)	1.422(-03)	1.339(-03)	
4 – 21	981.153	1.120(07)	7.761(06)	5.01(06)	6.464(-03)	4.476(-03)	2.904(-03)	
5 – 21	1022.589	4.986(06)	1.343(07)	1.08(07)	3.127(-03)	8.554(-03)	6.902(-03)	
6 – 21	1028.103	1.619(07)	2.197(06)		1.026(-02)	1.348(-03)		
7 – 21	1174.254	5.806(08)	2.535(08)	2.33(08)	4.801(-01)	2.008(-01)	1.853(-01)	2.24(-01)
8 – 21	1179.334	4.876(07)	4.094(08)	4.31(08)	4.067(-02)	3.538(-01)	3.741(-01)	3.42(-01)
9 – 21	2076.504	4.517(07)	4.361(07)	4.31(07)	1.168(-01)	1.018(-01)	1.002(-01)	
10 – 21	2094.047	5.294(06)	3.415(06)	3.31(06)	1.392(-02)	7.996(-03)	7.726(-03)	
1 – 22	92.226	2.083(10)	1.964(10)	1.96(10)	5.314(-02)	4.908(-02)	4.920(-02)	6.70(-02)
2 – 22	92.468	1.110(10)	1.232(10)	1.23(10)	2.845(-02)	3.108(-02)	3.097(-02)	4.26(-02)
3 – 23	146.805	5.237(06)	1.548(05)		6.769(-05)	1.968(-06)		
4 – 23	949.626	7.718(08)	6.774(08)	6.81(08)	4.174(-01)	3.808(-01)	3.837(-01)	3.48(-01)
5 – 23	988.389	3.575(08)	3.063(08)	3.08(08)	2.095(-01)	1.899(-01)	1.909(-01)	1.89(-01)
6 – 23	993.539	5.751(08)	5.521(08)	5.52(08)	3.405(-01)	3.301(-01)	3.303(-01)	3.30(-01)
7 – 23	1129.379	4.435(06)	4.529(05)	5.45(04)	3.393(-03)	3.484(-04)	4.197(-05)	
8 – 23	1134.078	3.772(06)	7.482(06)	5.32(06)	2.909(-03)	6.270(-03)	4.456(-03)	
9 – 23	1940.178	1.976(06)	1.302(06)		4.461(-03)	2.892(-03)		
10 – 23	1955.485	2.723(04)	9.887(04)		6.245(-05)	2.200(-04)		
3 – 24	146.615	4.880(07)	2.590(07)		3.145(-04)	1.644(-04)		
5 – 24	979.803	4.553(07)	2.065(06)		1.311(-02)	6.328(-04)		
6 – 24	984.864	1.963(03)	3.411(06)		5.710(-07)	1.008(-03)		
7 – 24	1118.182	2.447(08)	1.833(08)		9.173(-02)	6.964(-02)		
8 – 24	1122.788	7.678(08)	6.707(08)		2.902(-01)	2.772(-01)		
10 – 24	1922.160	1.678(07)	2.055(07)		1.859(-02)	2.237(-02)		
5 – 25	735.260	4.657(06)			2.265(-03)			
6 – 25	761.314	5.428(05)	1.357(04)	1.51(04)	2.830(-04)	7.164(-06)	8.035(-06)	
7 – 25	838.603	7.411(04)	7.983(04)		4.688(-05)	5.100(-05)		
9 – 25	1215.905	8.749(07)	7.805(07)	7.65(07)	1.163(-01)	1.035(-01)	1.020(-01)	1.09(-01)
10 – 25	1221.899	7.763(08)	7.612(08)	7.56(08)	1.043(+00)	1.011(+00)	1.006(+00)	1.11(+00)
4 – 26	733.553	8.310(05)	1.120(05)	1.20(05)	5.363(-04)	7.446(-05)	8.035(-05)	
9 – 26	1211.242	8.876(08)	8.628(08)	8.56(08)	1.562(+00)	1.501(+00)	1.499(+00)	1.64(+00)
3 – 27	138.443	1.456(03)	4.078(06)	4.89(06)	1.674(-08)	4.622(-05)		
4 – 27	682.827	3.924(05)	6.054(04)	6.24(04)	1.097(-04)	1.749(-05)	1.811(-05)	
5 – 27	702.641	1.011(06)	5.116(-1)	1.89(00)	2.994(-04)	1.584(-10)	5.902(-10)	
6 – 27	705.240	1.533(06)	1.283(06)	4.40(05)	4.573(-04)	1.294(-04)	1.339(-04)	
7 – 27	771.072	1.238(06)	1.967(07)	2.00(07)	4.413(-04)	7.076(-03)	7.244(-03)	
8 – 27	773.259	5.680(06)	5.306(06)	5.19(06)	2.037(-03)	2.024(-03)	1.995(-03)	
9 – 27	1078.900	1.254(08)	7.247(07)	7.17(07)	8.756(-02)	5.049(-02)	5.023(-02)	
10 – 27	1083.616	1.118(09)	1.117(09)	1.11(09)	7.875(-01)	7.792(-01)	7.798(-01)	8.03(-01)
4 – 28	679.840	2.305(07)	4.734(05)	4.88(05)	9.584(-03)	2.040(-04)	2.118(-04)	

Table 2. *Continued.*

<i>Transition</i>	$\lambda(\text{\AA})$	$A_{ki}(s^{-1})$			<i>gf</i>			
		<i>present</i>	<i>FF</i>	<i>NIST</i>	<i>present</i>	<i>FF</i>	<i>NIST</i>	<i>CT</i>
6 – 28	702.055	4.910(06)	5.481(03)	4.62(03)	2.177(–03)	2.467(–06)	2.094(–06)	
7 – 28	767.266	6.267(06)	1.070(07)	1.05(07)	3.319(–03)	5.740(–03)	5.675(–03)	
9 – 28	1071.462	1.150(09)	1.100(09)	1.10(09)	1.187(+00)	1.140(+00)	1.140(+00)	1.17(+00)
10 – 28	1076.114	1.288(08)	1.137(08)	1.13(08)	1.342(–01)	1.179(–01)	1.174(–01)	1.18(–01)
3 – 29	135.238	5.172(08)	7.112(08)	7.11(08)	5.673(–03)	7.758(–03)	7.762(–03)	
4 – 29	611.374	2.805(07)	5.525(05)	5.48(05)	6.287(–03)	1.326(–04)	1.327(–04)	
5 – 29	627.211	2.072(07)	1.148(05)	1.09(05)	4.888(–03)	2.936(–05)	2.818(–05)	
6 – 29	629.281	2.656(05)	1.930(07)	1.92(07)	6.306(–05)	4.820(–03)	4.841(–03)	
7 – 29	681.173	1.678(09)	1.402(09)	1.38(09)	4.670(–01)	4.104(–01)	4.083(–01)	4.32(–01)
8 – 29	682.880	3.009(08)	2.957(08)	2.92(08)	8.415(–02)	9.122(–02)	9.078(–02)	9.61(–02)
9 – 29	910.722	1.294(09)	1.235(09)	1.23(09)	6.436(–01)	6.498(–01)	6.486(–01)	
10 – 29	914.081	1.412(08)	5.801(07)	5.69(07)	7.075(–02)	3.054(–02)	3.013(–02)	
3 – 30	135.230	5.478(08)	8.058(08)	8.06(08)	3.004(–03)	4.368(–03)	4.355(–03)	
5 – 30	627.022	7.195(07)	3.778(06)	3.77(06)	8.482(–03)	4.686(–04)	4.720(–04)	
6 – 30	629.090	1.571(05)	4.630(06)	4.61(06)	1.864(–05)	5.608(–04)	5.636(–04)	
7 – 30	680.950	6.378(08)	4.582(08)	4.52(08)	8.868(–02)	6.496(–02)	6.411(–02)	6.83(–02)
8 – 30	682.655	1.200(09)	1.070(09)	1.06(09)	1.677(–01)	1.596(–01)	1.588(–01)	1.68(–01)
10 – 30	913.679	1.459(09)	1.448(09)	1.44(09)	3.653(–01)	3.649(–01)	3.647(–01)	3.73(–01)
3 – 31	130.708	8.779(08)	6.247(08)		8.995(–03)	6.224(–03)		
4 – 31	528.555	4.887(06)	1.410(05)		8.188(–04)	2.283(–05)		
5 – 31	540.350	3.953(06)	1.024(04)		6.922(–04)	1.745(–06)		
6 – 31	541.886	6.974(06)	2.069(06)		1.228(–03)	3.461(–04)		
7 – 31	579.929	2.418(08)	1.207(08)		4.877(–02)	2.297(–02)		
8 – 31	581.166	6.960(07)	2.686(07)		1.410(–02)	5.334(–03)		
9 – 31	738.377	1.559(05)	2.646(06)		5.098(–05)	7.962(–04)		
10 – 31	740.583	2.238(04)	1.572(06)		7.363(–06)	4.732(–04)		
3 – 32	130.562	8.400(08)	5.510(08)		4.293(–03)	2.744(–03)		
5 – 32	537.865	8.805(06)	6.903(05)		7.638(–04)	5.880(–05)		
6 – 32	539.386	1.317(03)	7.534(05)		1.149(–07)	6.296(–05)		
7 – 32	577.068	8.320(07)	7.216(07)		8.308(–03)	6.860(–03)		
8 – 32	578.292	1.931(08)	1.451(08)		1.937(–02)	1.438(–02)		
10 – 32	735.923	5.602(06)	1.894(06)		9.097(–04)	2.847(–04)		
1 – 34	85.232	8.382(06)	2.275(07)	2.30(07)	5.477(–05)	1.464(–04)	1.482(–04)	
1 – 35	85.224	9.086(05)	1.456(08)	1.45(08)	3.958(–06)	6.244(–04)	6.237(–04)	
2 – 35	85.431	6.482(07)	3.464(07)	3.50(07)	2.837(–04)	1.498(–04)	1.517(–04)	
1 – 36	85.181	8.300(07)	8.691(07)	8.61(07)	1.806(–04)	1.861(–04)	1.845(–04)	
2 – 36	85.387	1.621(08)	2.003(08)	1.99(08)	3.545(–04)	4.328(–04)	4.295(–04)	
1 – 38	84.422	8.666(07)	1.172(09)	1.18(09)	3.704(–04)	4.921(–03)	4.954(–03)	1.03(–01)
2 – 38	84.625	4.078(08)	2.408(09)	2.44(09)	1.751(–03)	1.020(–02)	1.035(–02)	1.96(–02)
1 – 41	84.133	8.295(08)	1.409(09)		1.761(–03)	2.958(–03)		
2 – 41	84.334	5.368(08)	1.743(07)		1.145(–03)	3.690(–05)		
1 – 42	84.066	4.006(08)	2.740(09)		1.698(–03)	1.148(–02)		
2 – 42	84.267	3.639(07)	5.164(08)		1.550(–04)	2.182(–03)		3.00(–04)
1 – 43	83.927	1.359(08)	3.789(08)		8.612(–04)	2.374(–03)		1.46(–02)
1 – 45	83.974	1.817(10)	2.211(10)		1.153(–01)	1.386(–01)		
1 – 46	83.742	3.143(10)	2.980(10)	2.99(10)	6.608(–02)	6.196(–02)	6.194(–02)	5.95(–02)
2 – 46	83.942	5.476(10)	4.368(10)	4.36(10)	1.157(–01)	9.156(–02)	9.141(–02)	8.40(–02)
1 – 47	83.546	6.063(10)	1.686(10)	1.77(10)	2.538(–01)	6.960(–02)	7.227(–02)	3.09(–01)
2 – 47	83.745	2.522(10)	9.938(10)	9.74(10)	1.061(–01)	4.138(–01)	4.064(–01)	4.00(–04)
1 – 48	83.678	4.790(10)	9.699(10)	9.60(10)	2.012(–01)	4.028(–01)	3.990(–01)	7.03(–02)
2 – 48	83.877	1.934(11)	9.296(10)	9.47(10)	8.162(–01)	3.894(–01)	3.981(–01)	8.26(–01)
1 – 49	83.595	2.281(11)	2.341(11)	2.34(11)	1.434(+00)	1.545(+00)	1.452(+00)	1.27(+00)
1 – 52	81.031	3.016(11)	2.850(11)	2.76(11)	5.939(–01)	5.556(–01)	5.395(–01)	6.00(–01)
2 – 52	81.218	7.742(10)	7.643(10)	8.45(10)	1.531(–01)	1.502(–01)	1.663(–01)	2.13(–01)
1 – 53	80.984	3.209(11)	2.749(11)	2.74(11)	1.262(+00)	1.068(+00)	1.069(+00)	1.33(+00)
2 – 53	81.171	3.233(10)	5.658(10)	5.67(10)	1.278(–01)	2.218(–01)	2.218(–01)	2.91(–01)
1 – 54	80.914	6.868(10)	6.732(10)	6.85(10)	1.348(–01)	1.306(–01)	1.333(–01)	2.11(–01)
2 – 54	81.100	2.860(11)	2.804(11)	2.78(11)	5.640(–01)	5.484(–01)	5.457(–01)	6.27(–01)

Table 2. Continued.

Transition	$\lambda(\text{\AA})$	$A_{ki}(s^{-1})$			gf			
		<i>present</i>	<i>FF</i>	<i>NIST</i>	<i>present</i>	<i>FF</i>	<i>NIST</i>	<i>CT</i>
1 – 56	80.844	3.445(10)	6.766(10)		2.025(–01)	3.939(–01)		7.83(–02)
1 – 57	80.800	1.848(11)	1.335(11)	1.31(11)	1.085(+00)	7.764(–01)	7.603(–01)	1.59(+00)
1 – 58	80.755	1.352(10)	3.492(10)	3.50(10)	5.289(–02)	1.351(–01)	1.355(–01)	1.97(–01)
2 – 58	80.941	1.969(11)	1.891(11)	1.89(11)	7.735(–01)	7.380(–01)	7.362(–01)	1.01(+00)
1 – 59	78.069	8.919(09)	7.731(09)	7.74(09)	3.260(–02)	2.776(–02)	2.779(–02)	
2 – 59	78.242	4.642(10)	5.577(10)	5.57(10)	1.704(–01)	2.018(–01)	2.018(–01)	2.72(–01)
1 – 60	78.025	4.737(10)	5.054(10)	5.05(10)	2.594(–01)	2.723(–01)	2.722(–01)	3.75(–01)
1 – 61	76.060	2.957(07)			1.539(–04)			
1 – 62	75.899	3.236(09)			5.589(–03)			
2 – 62	76.063	6.405(09)			1.111(–02)			
1 – 63	75.797	1.243(09)			4.281(–03)			1.14(–02)
2 – 63	75.961	2.661(08)			9.209(–04)			
1 – 64	75.676	2.243(10)		1.24(10)	7.702(–02)		4.197(–02)	4.21(–02)
2 – 64	75.839	4.741(09)		2.11(09)	1.635(–02)		7.194(–03)	7.20(–03)
1 – 65	75.583	5.689(09)			9.746(–03)			
2 – 65	75.746	1.202(10)			2.069(–02)			
4 – 66	278.937	1.029(10)			7.204(–01)			
6 – 66	282.606	2.931(09)			2.106(–01)			
7 – 66	292.617	2.511(07)			1.934(–03)			
9 – 66	328.147	5.179(07)			5.016(–03)			
10 – 66	328.582	6.473(03)			6.287(–07)			
3 – 67	107.011	3.996(06)			2.744(–05)			
4 – 67	278.853	6.399(09)			2.984(–01)			
5 – 67	282.101	3.730(09)			1.780(–01)			
6 – 67	282.519	1.629(09)			7.796(–02)			
7 – 67	292.524	1.005(07)			5.159(–04)			
8 – 67	292.839	4.215(08)			2.168(–02)			
9 – 67	328.031	2.309(07)			1.490(–03)			
10 – 67	328.466	2.775(06)			1.796(–04)			
3 – 68	106.811	3.368(06)			1.152(–05)			
5 – 68	280.715	1.075(09)			2.539(–02)			
6 – 68	281.129	1.059(10)			2.511(–01)			
7 – 68	291.034	3.005(07)			7.632(–04)			
8 – 68	291.345	6.976(07)			1.776(–03)			
10 – 68	326.587	8.116(06)			2.596(–04)			
4 – 69	273.806	3.264(09)			2.935(–01)			
9 – 69	321.069	7.827(06)			9.678(–04)			
3 – 70	105.978	6.730(03)			2.266(–08)			
5 – 70	275.031	3.121(09)			7.079(–02)			
6 – 70	275.428	3.863(02)			8.788(–09)			
7 – 70	284.929	8.093(04)			1.970(–06)			
8 – 70	285.227	1.165(08)			2.841(–03)			
10 – 70	318.919	1.142(04)			3.482(–07)			
3 – 71	105.843	1.511(06)			1.011(–05)			
4 – 71	271.056	9.192(06)			4.050(–04)			
5 – 71	274.125	1.417(09)			6.385(–02)			
6 – 71	274.519	1.151(09)			5.201(–02)			
7 – 71	283.956	3.861(04)			1.867(–06)			
8 – 71	284.252	2.438(08)			1.181(–02)			
9 – 71	317.295	4.312(06)			2.603(–04)			
10 – 71	317.701	6.615(04)			4.004(–06)			
4 – 72	270.433	5.068(07)			3.334(–03)			
6 – 72	273.880	1.299(09)			8.765(–02)			
7 – 72	283.272	2.124(09)			1.533(–01)			
9 – 72	316.441	3.720(04)			3.351(–06)			
10 – 72	316.845	3.494(05)			3.155(–05)			
4 – 73	271.104	2.072(08)			1.370(–02)			
6 – 73	274.569	1.876(09)			1.272(–01)			

Table 2. *Continued.*

<i>Transition</i>	$\lambda(\text{\AA})$	$A_{ki}(s^{-1})$			<i>gf</i>			
		<i>present</i>	<i>FF</i>	<i>NIST</i>	<i>present</i>	<i>FF</i>	<i>NIST</i>	<i>CT</i>
7 – 73	284.009	8.893(08)			6.453(–02)			
9 – 73	317.361	2.303(06)			2.086(–04)			
10 – 73	317.768	6.699(06)			6.085(–04)			
3 – 74	105.742	2.059(05)			1.381(–06)			
4 – 74	270.396	1.558(08)			6.832(–03)			
5 – 74	273.449	5.931(08)			2.660(–02)			
6 – 74	273.842	6.104(05)			2.745(–05)			
7 – 74	283.232	3.949(08)			1.900(–02)			
8 – 74	283.526	2.129(09)			1.026(–01)			
9 – 74	316.390	1.947(06)			1.169(–04)			
10 – 74	316.795	1.613(06)			9.709(–05)			
3 – 75	105.683	1.462(07)			4.896(–05)			
5 – 75	273.056	1.449(06)			3.239(–05)			
6 – 75	273.447	1.060(07)			2.376(–04)			
7 – 75	282.809	2.598(09)			6.230(–02)			
8 – 75	283.103	5.264(07)			1.265(–03)			
10 – 75	316.266	4.386(08)			1.315(–02)			
3 – 76	105.361	2.021(06)			1.345(–05)			
4 – 76	267.917	3.085(08)			1.328(–02)			
5 – 76	270.915	1.073(09)			4.722(–02)			
6 – 76	271.300	1.127(09)			4.973(–02)			
7 – 76	280.513	1.603(07)			7.565(–04)			
8 – 76	280.802	3.923(07)			1.855(–03)			
9 – 76	313.002	1.264(06)			7.425(–05)			
10 – 76	313.398	1.091(06)			6.425(–05)			
3 – 77	104.974	4.741(07)			3.133(–04)			
4 – 77	265.429	3.542(06)			1.497(–04)			
5 – 77	268.371	6.593(07)			2.848(–03)			
6 – 77	268.750	7.602(06)			3.293(–04)			
7 – 77	277.787	1.359(09)			6.288(–02)			
8 – 77	278.07	1.709(08)			7.925(–03)			
9 – 77	309.612	1.217(09)			6.997(–02)			
10 – 77	309.999	1.274(08)			7.344(–03)			
3 – 78	104.935	3.845(07)			1.270(–04)			
5 – 78	268.119	1.251(08)			2.696(–03)			
6 – 78	268.497	1.917(07)			4.144(–04)			
7 – 78	277.517	1.251(06)			2.888(–05)			
8 – 78	277.800	1.619(09)			3.747(–02)			
10 – 78	309.663	8.910(08)			2.562(–02)			
1 – 79	73.253	9.110(09)		8.24(09)	4.398(–02)		3.935(–02)	3.94(–02)
1 – 80	73.232	1.305(09)			4.198(–03)			
2 – 80	73.385	7.299(09)			2.357(–02)			
1 – 82	72.246	2.920(08)			1.371(–03)			
1 – 83	72.222	1.216(02)			3.802(–10)			
2 – 83	72.371	2.423(08)			7.611(–04)			
1 – 84	72.175	5.005(08)			7.818(–04)			
2 – 84	72.323	9.647(08)			1.513(–03)			
1 – 87	71.976	2.262(10)			1.054(–01)			1.89(–01)
1 – 88	71.976	1.382(08)			4.293(–04)			
2 – 88	72.124	6.586(08)			2.055(–03)			1.03(–01)
1 – 89	71.910	2.267(09)			3.515(–03)			
2 – 89	72.057	3.055(09)			4.756(–03)			
1 – 90	71.845	1.208(09)			3.740(–03)			2.35(–02)
2 – 90	71.991	2.033(07)			6.318(–05)			2.00(–04)
1 – 91	71.742	1.462(09)			6.769(–03)			1.96(–02)
1 – 92	71.793	1.906(10)			8.839(–02)			
1 – 94	71.761	2.760(10)		2.19(10)	4.261(–02)		3.341(–02)	3.34(–02)
2 – 94	71.907	5.142(10)		3.56(10)	7.972(–02)		5.457(–02)	5.47(–02)
1 – 95	71.761	2.760(10)		7.20(10)	4.261(–02)			
2 – 95	71.907	5.142(10)		3.26(07)	7.972(–02)		1.000(–04)	1.00(–04)

Table 3. This table gives electron-, proton and singly-charged helium-impact broadening parameters for Si VI lines calculated using SUPERSTRUCTURE oscillator strength, for a perturber density of 10^{17} cm^{-3} and temperature of 50000 to 800000 K. Transitions, averaged wavelength for the multiplet (in Å) and parameter C are also given. This parameter when divided with the corresponding Stark width gives an estimate for the maximal perturber density for which the line may be treated as isolated. w_e : electron-impact full Stark width at half maximum, d_e : electron-impact Stark shift, w_{H+} : proton-impact full Stark width at half maximum, d_{H+} : proton-impact Stark shift, w_{He+} : singly charged helium-impact full Stark width at half maximum, d_{He+} : singly charged helium-impact Stark shift. w_{MSE} : electron-impact full Stark width at half maximum calculated by Dimitrijević (1993) using modified semiempirical formula (Dimitrijević & Konjević 1980).

transition	T(K)	w_e	d_e	w_{H+}	d_{H+}	w_{He+}	d_{He+}	w_{MSE}
SiVI 3S-3P 1226.7 Å C= 0.11E+21	50000.	0.750E-02	-0.577E-04	0.360E-04	-0.260E-04	0.687E-04	-0.500E-04	0.415E-02
	100000.	0.532E-02	-0.739E-04	0.897E-04	-0.516E-04	0.173E-03	-0.103E-03	0.294E-02
	200000.	0.387E-02	-0.784E-04	0.177E-03	-0.920E-04	0.344E-03	-0.185E-03	0.212E-02
	400000.	0.291E-02	-0.100E-03	0.269E-03	-0.139E-03	0.529E-03	-0.280E-03	0.169E-02
	800000.	0.227E-02	-0.888E-04	0.347E-03	-0.189E-03	0.693E-03	-0.384E-03	0.147E-02
SiVI 3S-3P 1187.2 Å C= 0.67E+20	50000.	0.681E-02	-0.660E-04	0.346E-04	-0.294E-04	0.660E-04	-0.566E-04	0.375E-02
	100000.	0.486E-02	-0.841E-04	0.866E-04	-0.582E-04	0.167E-03	-0.116E-03	0.265E-02
	200000.	0.354E-02	-0.890E-04	0.171E-03	-0.102E-03	0.335E-03	-0.205E-03	0.191E-02
	400000.	0.267E-02	-0.109E-03	0.262E-03	-0.150E-03	0.517E-03	-0.304E-03	0.152E-02
	800000.	0.208E-02	-0.993E-04	0.340E-03	-0.203E-03	0.678E-03	-0.412E-03	0.132E-02
SiVI 3S'-3P' 1228.8 Å C= 0.72E+20	50000.	0.716E-02	-0.644E-04	0.471E-04	-0.212E-04	0.899E-04	-0.409E-04	0.389E-02
	100000.	0.509E-02	-0.599E-04	0.113E-03	-0.424E-04	0.219E-03	-0.842E-04	0.275E-02
	200000.	0.370E-02	-0.615E-04	0.213E-03	-0.771E-04	0.416E-03	-0.155E-03	0.198E-02
	400000.	0.278E-02	-0.770E-04	0.314E-03	-0.119E-03	0.618E-03	-0.241E-03	0.158E-02
	800000.	0.216E-02	-0.691E-04	0.389E-03	-0.164E-03	0.774E-03	-0.331E-03	0.137E-02
SiVI 3S'-3P' 1087.4 Å C= 0.56E+20	50000.	0.572E-02	-0.376E-04	0.399E-04	-0.131E-04	0.762E-04	-0.252E-04	0.312E-02
	100000.	0.408E-02	-0.358E-04	0.948E-04	-0.263E-04	0.183E-03	-0.521E-04	0.220E-02
	200000.	0.297E-02	-0.371E-04	0.176E-03	-0.487E-04	0.344E-03	-0.978E-04	0.158E-02
	400000.	0.223E-02	-0.460E-04	0.256E-03	-0.774E-04	0.505E-03	-0.156E-03	0.126E-02
	800000.	0.174E-02	-0.413E-04	0.313E-03	-0.107E-03	0.623E-03	-0.216E-03	0.109E-02
SiVI 3S-3P 1314.8 Å C= 0.13E+21	50000.	0.842E-02	-0.107E-03	0.361E-04	-0.374E-04	0.690E-04	-0.721E-04	0.436E-02
	100000.	0.598E-02	-0.118E-03	0.927E-04	-0.740E-04	0.179E-03	-0.147E-03	0.309E-02
	200000.	0.434E-02	-0.116E-03	0.189E-03	-0.129E-03	0.368E-03	-0.260E-03	0.224E-02
	400000.	0.326E-02	-0.148E-03	0.295E-03	-0.190E-03	0.582E-03	-0.384E-03	0.180E-02
	800000.	0.254E-02	-0.134E-03	0.392E-03	-0.256E-03	0.784E-03	-0.519E-03	0.155E-02
SiVI 3S-3P 1145.4 Å C= 0.10E+21	50000.	0.656E-02	-0.682E-04	0.295E-04	-0.254E-04	0.563E-04	-0.488E-04	0.343E-02
	100000.	0.466E-02	-0.797E-04	0.745E-04	-0.503E-04	0.144E-03	-0.999E-04	0.242E-02
	200000.	0.338E-02	-0.787E-04	0.149E-03	-0.887E-04	0.290E-03	-0.178E-03	0.175E-02
	400000.	0.254E-02	-0.102E-03	0.229E-03	-0.132E-03	0.452E-03	-0.267E-03	0.141E-02
	800000.	0.198E-02	-0.909E-04	0.300E-03	-0.179E-03	0.599E-03	-0.364E-03	0.122E-02
SiVI 2P-3S 100.2 Å C= 0.73E+18	50000.	0.209E-04	-0.851E-06	0.885E-08	0.227E-06	0.169E-07	0.438E-06	0.154E-04
	100000.	0.138E-04	0.531E-06	0.665E-07	0.449E-06	0.128E-06	0.891E-06	0.109E-04
	200000.	0.976E-05	0.815E-06	0.288E-06	0.780E-06	0.571E-06	0.157E-05	0.791E-05
	400000.	0.740E-05	0.981E-06	0.709E-06	0.114E-05	0.143E-05	0.231E-05	0.628E-05
	800000.	0.577E-05	0.918E-06	0.131E-05	0.153E-05	0.262E-05	0.311E-05	0.541E-05
SiVI 2P-3D 83.8 Å C= 0.77E+18	50000.	0.267E-04	-0.113E-05	0.147E-06	-0.328E-07	0.280E-06	-0.631E-07	0.194E-04
	100000.	0.179E-04	-0.289E-06	0.365E-06	-0.663E-07	0.703E-06	-0.131E-06	0.137E-04
	200000.	0.130E-04	-0.490E-07	0.715E-06	-0.128E-06	0.139E-05	-0.257E-06	0.969E-05
	400000.	0.967E-05	-0.134E-06	0.108E-05	-0.221E-06	0.212E-05	-0.444E-06	0.747E-05
	800000.	0.741E-05	-0.802E-07	0.139E-05	-0.321E-06	0.277E-05	-0.647E-06	0.631E-05
SiVI 2P-3D 83.8 Å C= 0.35E+18	50000.	0.266E-04	-0.116E-05	0.147E-06	-0.165E-07	0.280E-06	-0.318E-07	0.193E-04
	100000.	0.174E-04	-0.200E-06	0.364E-06	-0.335E-07	0.701E-06	-0.664E-07	0.137E-04
	200000.	0.125E-04	0.533E-07	0.712E-06	-0.662E-07	0.139E-05	-0.132E-06	0.967E-05
	400000.	0.929E-05	-0.605E-08	0.107E-05	-0.121E-06	0.211E-05	-0.243E-06	0.748E-05
	800000.	0.709E-05	0.492E-07	0.139E-05	-0.188E-06	0.275E-05	-0.380E-06	0.631E-05

Table 3. *Continued.*

transition	T(K)	w_e	d_e	w_{H^+}	d_{H^+}	w_{He^+}	d_{He^+}	w_{MSE}
SiVI 2P-3S'	50000.	0.202E-04	-0.613E-06	0.106E-07	0.247E-06	0.202E-07	0.475E-06	0.139E-04
96.7 A	100000.	0.135E-04	0.635E-06	0.787E-07	0.484E-06	0.152E-06	0.961E-06	0.984E-05
C= 0.45E+18	200000.	0.958E-05	0.879E-06	0.317E-06	0.831E-06	0.629E-06	0.167E-05	0.712E-05
	400000.	0.728E-05	0.105E-05	0.752E-06	0.121E-05	0.151E-05	0.244E-05	0.564E-05
	800000.	0.570E-05	0.993E-06	0.139E-05	0.158E-05	0.278E-05	0.321E-05	0.486E-05
SiVI 2P-3D'	50000.	0.277E-04	-0.116E-05	0.212E-06	-0.144E-07	0.405E-06	-0.277E-07	0.178E-04
81.2 A	100000.	0.176E-04	-0.202E-06	0.504E-06	-0.291E-07	0.972E-06	-0.578E-07	0.126E-04
C= 0.58E+18	200000.	0.127E-04	0.363E-07	0.935E-06	-0.577E-07	0.183E-05	-0.115E-06	0.902E-05
	400000.	0.937E-05	-0.255E-07	0.136E-05	-0.106E-06	0.268E-05	-0.213E-06	0.710E-05
	800000.	0.716E-05	0.289E-07	0.166E-05	-0.166E-06	0.330E-05	-0.336E-06	0.612E-05
SiVI 2P-3D'	50000.	0.273E-04	-0.119E-05	0.214E-06	-0.231E-07	0.408E-06	-0.445E-07	0.179E-04
81.2 A	100000.	0.174E-04	-0.260E-06	0.508E-06	-0.468E-07	0.981E-06	-0.928E-07	0.126E-04
C= 0.59E+18	200000.	0.125E-04	-0.196E-07	0.942E-06	-0.916E-07	0.184E-05	-0.183E-06	0.904E-05
	400000.	0.923E-05	-0.845E-07	0.137E-05	-0.161E-06	0.270E-05	-0.324E-06	0.710E-05
	800000.	0.704E-05	-0.422E-07	0.167E-05	-0.239E-06	0.332E-05	-0.483E-06	0.610E-05
SiVI 2P-3D'	50000.	0.270E-04	-0.107E-05	0.219E-06	-0.148E-07	0.419E-06	-0.285E-07	0.179E-04
81.0 A	100000.	0.175E-04	-0.202E-06	0.520E-06	-0.299E-07	0.100E-05	-0.594E-07	0.127E-04
C= 0.60E+18	200000.	0.126E-04	0.317E-07	0.960E-06	-0.592E-07	0.187E-05	-0.118E-06	0.905E-05
	400000.	0.935E-05	-0.301E-07	0.139E-05	-0.109E-06	0.274E-05	-0.218E-06	0.711E-05
	800000.	0.714E-05	0.195E-07	0.169E-05	-0.170E-06	0.336E-05	-0.343E-06	0.609E-05
SiVI 3S'-3P'	50000.	0.439E-02	-0.460E-04	0.328E-04	-0.168E-04	0.626E-04	-0.324E-04	0.241E-02
918.8 A	100000.	0.314E-02	-0.597E-04	0.773E-04	-0.333E-04	0.149E-03	-0.662E-04	0.171E-02
C= 0.40E+20	200000.	0.229E-02	-0.606E-04	0.142E-03	-0.586E-04	0.278E-03	-0.118E-03	0.123E-02
	400000.	0.173E-02	-0.737E-04	0.206E-03	-0.869E-04	0.407E-03	-0.176E-03	0.976E-03
	800000.	0.135E-02	-0.698E-04	0.252E-03	-0.118E-03	0.500E-03	-0.239E-03	0.845E-03
Si VI 3S-3P	50000.	0.510E-02	-0.414E-04	0.244E-04	-0.159E-04	0.465E-04	-0.306E-04	0.263E-02
995.6 A	100000.	0.362E-02	-0.514E-04	0.604E-04	-0.317E-04	0.116E-03	-0.630E-04	0.186E-02
C= 0.75E+20	200000.	0.263E-02	-0.509E-04	0.118E-03	-0.569E-04	0.230E-03	-0.114E-03	0.134E-02
	400000.	0.198E-02	-0.655E-04	0.179E-03	-0.864E-04	0.352E-03	-0.175E-03	0.107E-02
	800000.	0.155E-02	-0.589E-04	0.230E-03	-0.118E-03	0.458E-03	-0.240E-03	0.923E-03